DOI: 10.13009/EUCASS2017-424

Experimental Research of the Inward-Turning Intake Starting at TsAGI T-116 Wind Tunnel within the International HEXAFLY-INT Project

Anatoly A. Gubanov, Natalia V. Guryleva*, Michail A. Ivankin*, Vadim A Talyzin*, Nina V. Voevodenko* and Valentina A. Yakovleva**

**Central Aerohydrodynamic Institute named after Professor N.E. Zhukovsky (TsAGI),*

1 Zhukovsky Street, Zhukovsky Moscow Region, 140180 Russian Federation

Abstract
The main results of the experimental investigation on the mass flow rate performance for an inward-turning intake are presented. The model tests have been provided at Mach numbers M = 6, 7 and 8 at the TsAGI wind tunnel T-116. It was shown that the intake starting significantly depends from the state of the boundary layer on the intake compression surface. For the model with transition grit installed on the intake internal surface, the complex hysteresis pattern of the intake mass flow rate dependence from angle-of-attack was observed.

1. Introduction

The research refers to the configuration of the inward-turning dorsal mounted intake which is supposed to be used for a high-speed passenger vehicle LAPCAT MR-2 with cruise speed corresponding to Mach number M=8. The conceptual design of the vehicle had been developed within European Community (EU) co-funded projects: ATLLAS I & II, LAPCAT I & II [1][2][3]. The general view of the LAPCAT MR-2 vehicle taken from Ref. [2] is shown in Figure 1. The intake of the vehicle is of a stream-traced inward-turning type with an elliptical entrance located in a dorsal position at the forward part of the fuselage.

Figure 1: General view of the LAPCAT MR-2 passenger vehicle

The current International Project HEXAFLY-INT includes investigations of two different concepts of the experimental flight test vehicle EFTV of approximately 3 m length: the powered one, and the glider. The configuration of the EFTV powered option had been developed on the basis of the LAPCAT MR-2 vehicle by European Partners within a preceding project HEXAFLY [4]. Investigations on the EFTV powered concept are being

DOI: 10.13009/EUCASS2017-424

conducted in the HEXAFLY-INT Project just by Russian Partners. The Central Aerohydrodynamic Institute named after Professor N.E. Zhukovsky (TsAGI) provides, in particular, CFD and experimental research on aerodynamics of the EFTV powered vehicle, and the intake performance. The EFTV glider configuration is under development and investigation by all members of the HEXAFLY-INT Consortium including EU, Russian, and Australian Entities.

2. Description of the wind-tunnel and the test model

For experimental study of the EFTV powered option, an experimental test campaign was carried out by TsAGI in the supersonic and hypersonic wind tunnel T-116 characterized by a test chamber with a squared cross section of 2.35 m × 1 m × 1 m size. The wind tunnel is a blow-down type exhausting into the atmosphere by the aid of ejectors. The working gas is air. It allows providing different types of tests of vehicles and their components within a Mach number range from 1.8 to 10. The Reynolds number (referred to a model length of 1 m) varies from $2.5 \cdot 10^6$ to $42 \cdot 10^6$. The duration of wind tunnel runs is up to 7 minutes. To prevent condensation of the air components during tests, the wind tunnel is equipped with two types of electrical heaters dedicated to different Mach number ranges. The total temperature of the flow varies from 300 to 1075 K.

The universal aerodynamic model of the EFTV powered option was produced for tests in the wind tunnel T-116. The scale of the model having a length of about 1 m was 35 % to the real size of the vehicle. The model was made with the internal duct simulating the intake configuration up to its throat. The other parts of the duct were modified as compared to the real engine components. At some distance from the intake throat the duct was made with the expanding, and then with constant cross-sectional area. The nozzle of the model duct was composed of two parts having contracting and constant cross-sectional areas ensuring a uniform exit flow with sonic velocity. Such a configuration of the internal duct allows determining the intake mass flow rate and the nozzle exit flow momentum by measurement of total and static pressures and total temperature in the exit section of the nozzle by the special rake consisting of several total and static pressure probes and thermocouples. Composition of the aerodynamic model is shown in Figure 2. Configuration of the internal duct of the model and position of the measurement rake are shown in Figure 3.

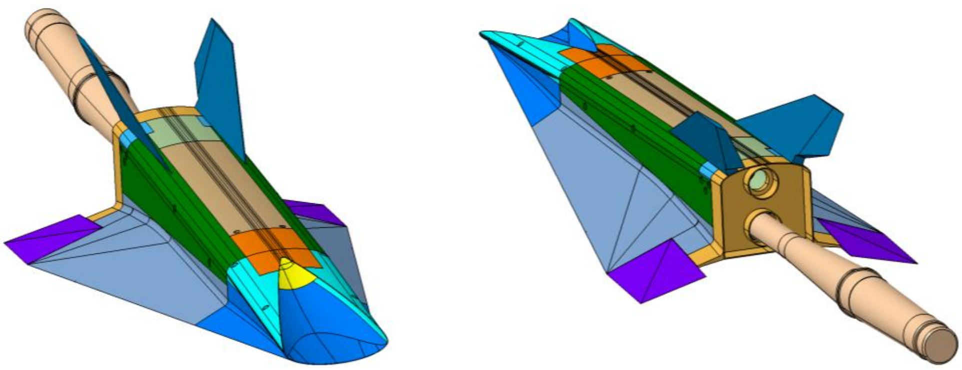

Figure 2: Composition of the EFTV powered option aerodynamic model

DOI: 10.13009/EUCASS2017-424

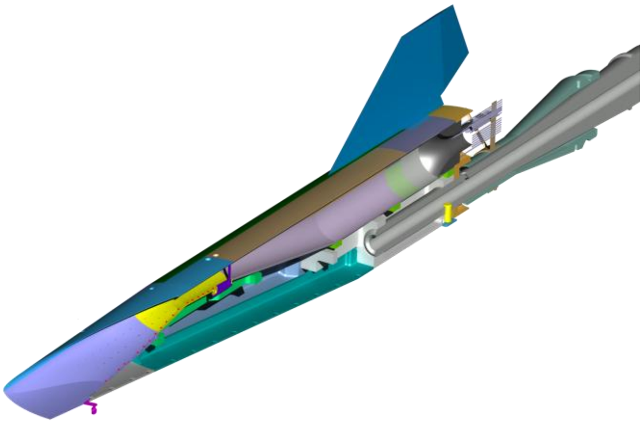

Figure 3: Configuration of the internal duct of the model and the measurement rake

In order to study the influence of the intake throat area on the intake starting performance, the model was manufactured with two variants of the intake throat: the original one corresponding to the EFTV configuration with the contraction ratio CR = 8.6, and a more expanded throat with CR = 7.4 (CR being the ratio of the intake capturing area to the area of the intake throat). These two variants of the intake throat were ensured by two replaceable inserts shown in Figures 2 and 3 by yellow color.

For tests on the exit flow measurement and balance tests, the model was installed in the wind tunnel on the conventional tail sting. For providing tests on throttling characteristics of the intake, the special adaptor was manufactured for installation of the model on special support system with throttling device. Position of the throttle was changed during the experiment. The photos of the model installed in the wind tunnel for aerodynamic tests and for intake tests are presented in Figure 4. The intake tests were made with the model installed in the overturned position. The nose part of the model installed on the throttling device was placed in front of the optical windows of the wind tunnel. It allowed making Schlieren pictures of the flow around the intake.

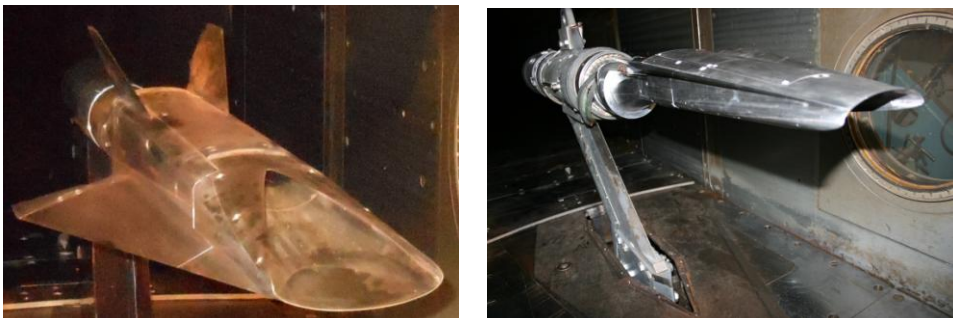

Figure 4: The model installed in T-116 on the tail sting (left) and on the throttling device (right)

3. The test campaign and the main results

The model was tested in the wind tunnel T-116 at Mach numbers 6, 7 and 8. The 1st series of tests was provided with the model installed on the tail sting with smooth intake surface – without any transition grit. The free-stream flow parameters realized in the working chamber of the wind tunnel during this test series are shown in Table 1. The Reynolds numbers realized in the tests fairly corresponded to the anticipated EFTV flight test conditions – the gliding phase of the flight test will start at an altitude of approximately 30 km.

DOI: 10.13009/EUCASS2017-424

Table 1: Free-stream flow parameters in T-116 during the 1st test series

M	**6.00**	**6.99**	**7.88**
P_0, atm	7.4	22	31.5
T_0, K	485	675	825
Re_{1m}*10^{-6}	6.32	7.66	5.92
Simulated flight altitudes (L=3 m):			
H, км	30.5	30	32.5

The tests showed that the intake with the original throat (CR = 8.6) did not start in the Mach number range M = 6 – 8 at any angle-of-attack, and the intake mass flow rate coefficient *f* was less than 0.6. At the same time, the intake with the expanded throat having a smooth internal surface (without a transition grit) started just in very limited range of the test regimes – at Mach number M = 8 and negative angles-of-attack $\alpha \leq -1°$. It was supposed that the problem of the intake starting occurred from laminar boundary layer on the intake internal surface which is less tolerant to positive longitudinal (stream vise) component of the pressure gradient as compared to turbulent boundary layer.

In order to study the effect numerically, CFD calculations of viscous flows around the intake were made with ANSYS FLUENT CFD Package with turbulent and laminar boundary layer settings. The results of CFD research and their comparison with the described above experimental data are presented in Refs. [5], [6] and [7]. For example, two flow-fields obtained by CFD at free-stream Mach number M = 7 and angle-of-attack α = 0 are presented in Figure 5. The Figure represents local Mach number distributions in the symmetry plane of the intake obtained for preliminarily set laminar and turbulent boundary layers. It is seen that the flow-fields differ dramatically: in the case of laminar boundary layer (the left picture) all the intake entrance area is covered by huge separation zone with subsonic flow (represented by blue color). The intake crotch can be seen as the dark point in the middle of the blue zone at the right side of the picture. The calculated mass flow rate coefficient of the intake in the case of laminar boundary layer was $f \approx 0.5$. If the boundary layer is pre-set as turbulent (the right picture) the separation zone is of significantly less size, and it covers just part of the intake entrance, though its height in the vicinity of the symmetry plane is maximal. The calculated intake mass flow rate coefficient for the case of turbulent boundary layer was $f \approx 0.95$. These CFD results supported the mentioned above suggestion that the cause of the intake unstart at the most test regimes considered lies in the laminar state of the boundary layer.

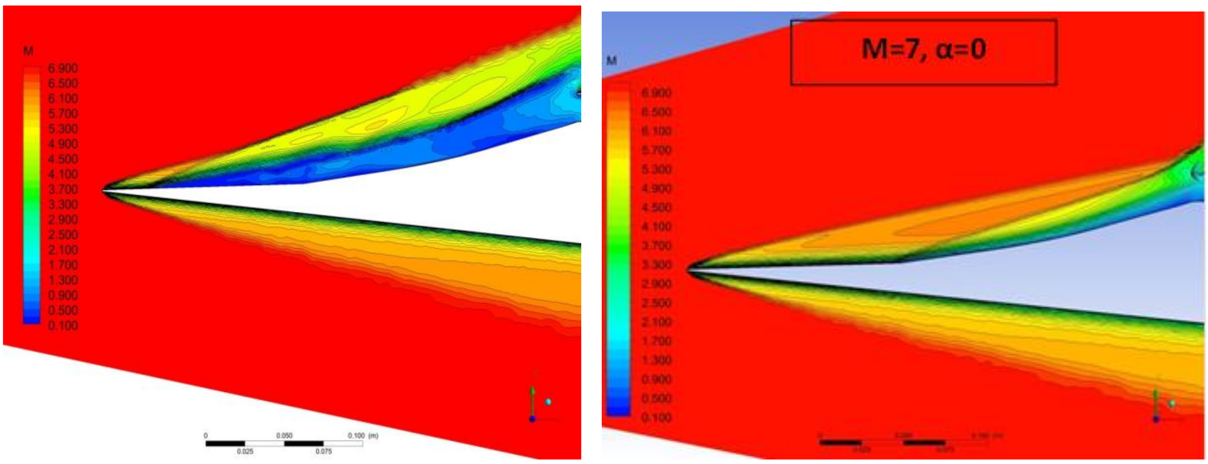

Figure 5: Local Mach number flow-fields for pre-set laminar (left) and turbulent (right) boundary layers

Laminar state of the boundary layer on the main part of the intake compression surface was also proved by special temperature measurement tests which allowed calculating the local Stanton numbers at three points on the intake surface [7]. These tests showed that boundary layer is laminar on the main part of the intake compression surface,

DOI: 10.13009/EUCASS2017-424

with trend to transitional state of the boundary layer in the part of the compression surface approaching to the intake throat.

In order to investigate possibilities of improvement the intake starting performance, the 2nd series of wind-tunnel tests was provided with different transition grits installed on the intake internal surface. The main results of the tests are briefly described in Refs. [6] and [7]. The variants of transition grits considered are shown in Figure 6.

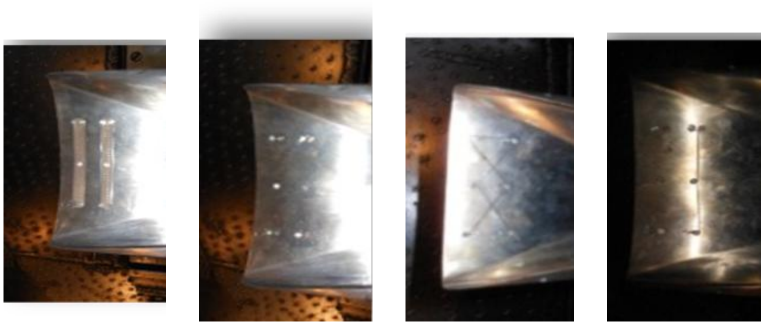

Variant 1 Variant 2 Variant 3 Variant 4

Figure 6: Different variants of the transition grit tested

The Variant 1 of the transition grit consisted of two curved plates with three rows of diamond-shaped roughness elements on each installed on the forward part of the intake surface at distances of 10 mm and 30 mm from the leading edge (LE) of the intake. The sketch of the plates is shown in Figure 7. The heights of the roughness elements were h = 0.75 mm for the 1st plate, and h = 1 mm for the 2nd one.

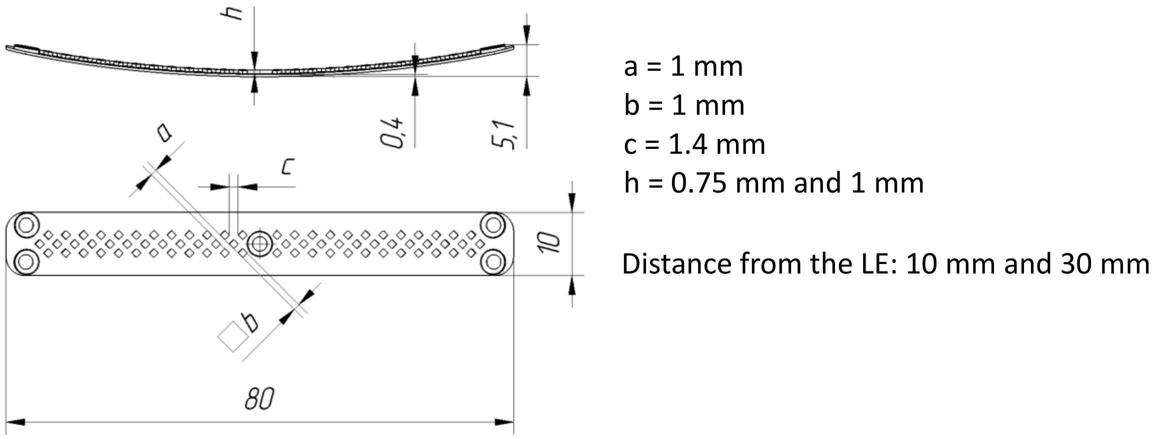

Figure 7: The sketch of transition grit components, Variant 1

Variant 2 of the transition grit consisted of 10 screw heads of countersunk shape with a height of 1.2 mm and 3.8 mm top diameter installed as shown on Figure 6 at distances of approximately 15 mm and 35 mm from the leading edge of the intake at three positions dispersed by the lateral co-ordinate (the same screws were used for installation of the plates of Variant 1 on the intake surface). Variants 3 and 4 of the transition grit were formed by adding wires of 0.5 mm diameter to the screw heads of Variant 2. At Variant 3, wires were installed between screw heads obliquely in the form of X crosses. At Variant 4, wires were installed between screws in the direction parallel to the leading edge of the intake.

The tests showed that the Variant 1 of the transition grit did not led to any improvement – the intake did not start even at negative angles-of-attack at Mach number M = 8, i.e. the situation became worthier as compared to the case of the intake with smooth internal surface. The reason of that, probably, was in small steps formed by the plates which led to initiated shock waves and reconstructed the whole picture of the flow. Oppositely, the tests showed that all the other variants of transition grit (from Variant 2 to Variant 4) led to significantly wider ranges of test conditions at which the intake started. The test results obtained at Mach numbers 7 and 8 in terms of the intake mass

DOI: 10.13009/EUCASS2017-424

flow rate coefficient *f* are shown in Figure 8. It is seen that the intake started (with high values of $f > 0.6$) at Mach number M = 7, Re = $7.22 \cdot 10^6$ at the angle-of-attack range $\alpha \leq 4°$. For less value of the Reynolds number (Re = $4.22 \cdot 10^6$) the range of the intake starting was slightly narrower: $\alpha < 3°$, but in any case the intake started in the vicinity of the vehicle design flight condition corresponded to $\alpha = 0$. At Mach number M = 8, the angle-of-attack range of the intake starting also became spread to $\alpha < 3°$ i.e. wider than the intake with a smooth surface. Low values of mass flow rate coefficient *f* (less than approximately 0.6) at higher angles-of-attack indicate absence of the intake starting.

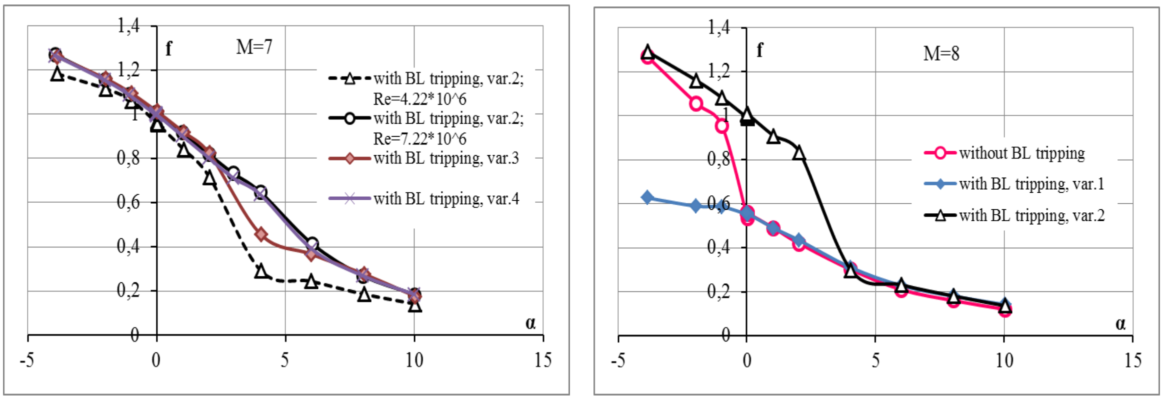

Figure 8: Experimental data on the intake mass flow rate coefficient f at Mach Numbers 7 and 8

All the results of the 2nd test series were obtained with the intake having an expanded throat area (CR = 7.6).

The aims of the 3rd test series of the aerodynamic model were to study more carefully the starting performance of the inward-turning intake with the expanded throat area and to examine whether transition grit helps to ensure starting of the intake with the original throat, CR = 8.6. The tests were provided with different histories of angles-of-attack change. The three curves of the intake mass flow rate dependencies from angle-of-attack of the model obtained at Mach number M = 7 are shown in Figure 9.

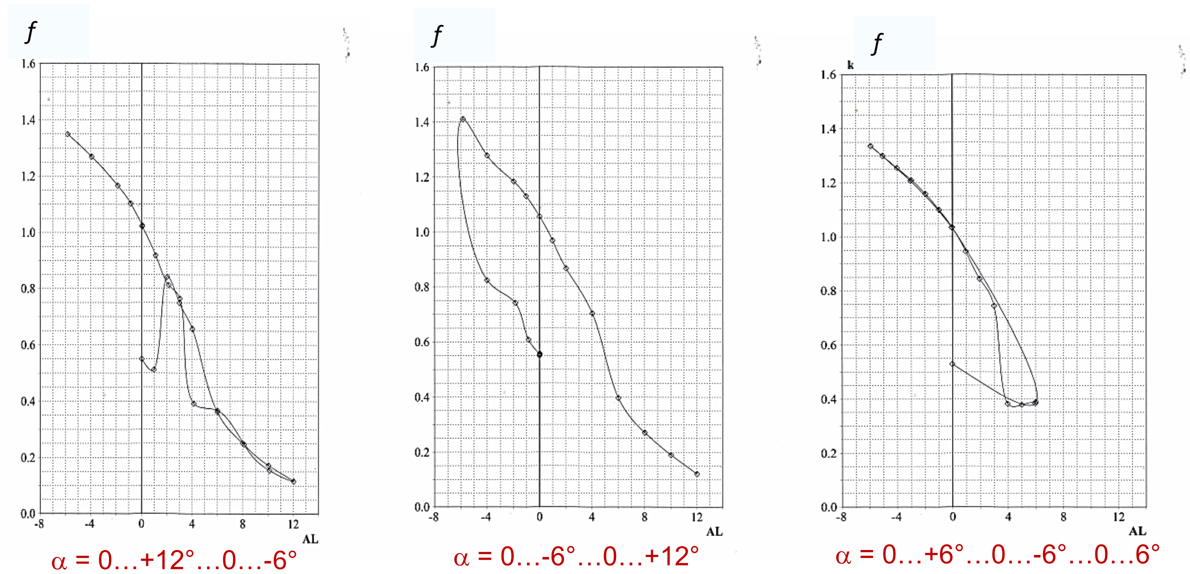

Figure 9: Dependencies of the intake mass flow rate coefficient from angle-of-attack change

It is seen that the intake starting significantly depends from the prehistory of the angle-of-attack change. In other words, the complex hysteresis pattern of the intake mass flow rate dependencies from angle-of-attack takes place. After the start of the flow regime in the wind tunnel, the intake of the model initially installed at $\alpha = 0$ was not started, but when the angle-of-attack changed to $\alpha = -6°$ or to $\alpha = +3°$, the intake became started, and it remained started when the angle-of-attack came back to $\alpha = 0$.

DOI: 10.13009/EUCASS2017-424

The similar pattern of the intake starting was observed during the special intake tests with the throttling device. The corresponding photos of the model and dependencies of the intake mass flow rate from angle-of-attack obtained at two different runs of tests are shown in Figure 10.

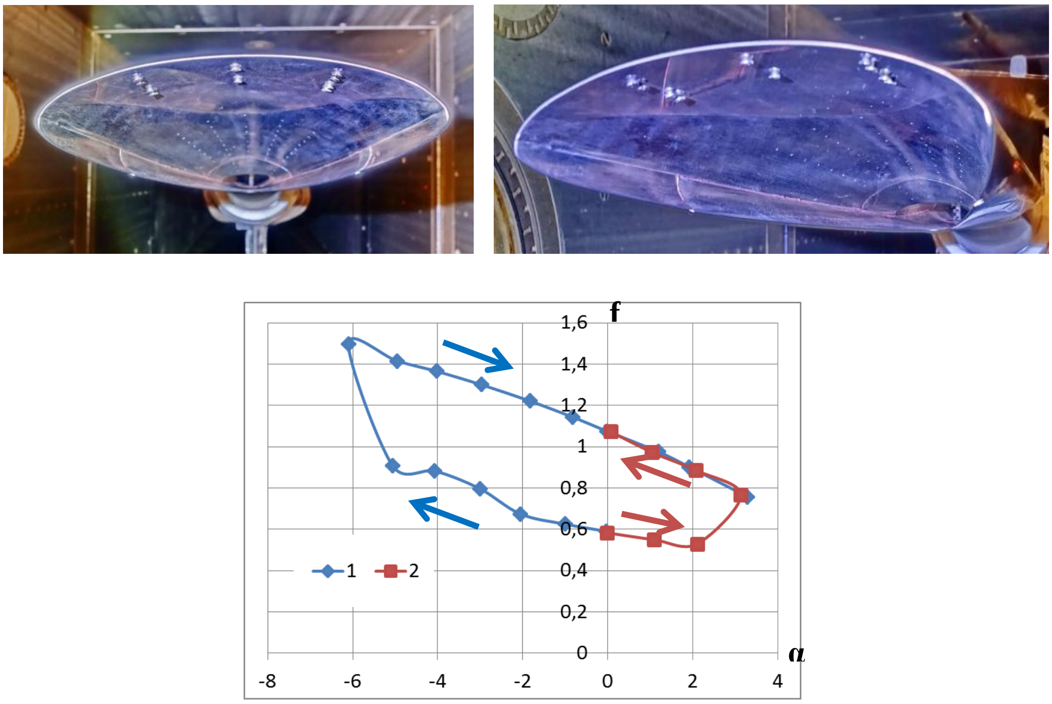

Figure 10: The photos of the intake model and the related starting performance of the intake, M = 7

The hysteresis pattern of the intake starting performance is quite similar to that shown above in Figure 9. Shlieren pictures of the flow obtained during the intake tests for unstarted and started intake are shown in Figure 11.

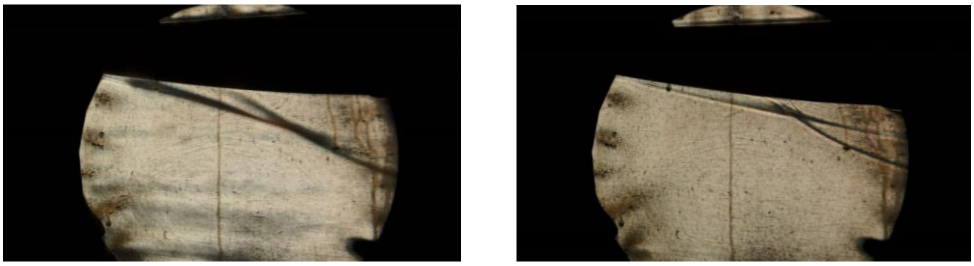

Figure 11: Shlieren pictures of the flow around unstarted (left) and started (right) intake, M = 7; α = 0

The left picture of the flow around unstarted intake displays much stronger bow shock wave which obviously means that more amount of compressed air passes away from the intake entrance than on the right picture. The cases of the started intake were detected again just with the expanded throat area. Wind tunnel tests showed also that the intake started at M = 7 just in the case when the screw heads were dispersed by the lateral co-ordinate. If the screw heads were installed just in the symmetry plane of the intake or, otherwise, just in the peripheral positions, the intake remained unstarted.

4. Conclusion

1. The complex hysteresis pattern of the intake starting performance strongly dependent from prehistory of angle-of-attack change was detected.
2. The start of the intake with the expanded throat area is possible just with the roughness elements dispersed along the lateral co-ordinate.
3. The problem on the intake starting with the original throat (CR = 8.4) needs further investigations.

DOI: 10.13009/EUCASS2017-424

References

[1] Meerts, C., and J. Steelant. 2013. Air intake design for the acceleration propulsion unit of the LAPCAT-MR2 hypersonic aircraft. In: *5th European Conference for Aeronautics and Space Sciences (EUCASS),* Munich, July 1 – 5.

[2] Steelant, J., and T. Langener. 2014. The LAPCAT-MR2 hypersonic cruiser concept. In: *29th Congress of the International Council of the Aeronautical Sciences (ICAS),* St. Petersburg, September 7 – 12.

[3] Steelant, J., R. Varvill, S. Defoort, K. Hannemann, and M. Marini. 2015. Achievements obtained for sustained hypersonic flight within the LAPCAT-II project”. In: *20th AIAA International Space Planes and Hypersonic Systems and Technologies Conference,* Glasgow, Scotland, July 6 – 9: AIAA 2015-3677.

[4] Steelant, J., T. Langener, F. Di Matteo, K. Hannemann, J. Riehmer, M. Kuhn, C. Dittert, F. Scheuerpflug, W. Jung, M. Marini, G. Pezzella, M. Cicala, and L. Serre. 2015. Conceptual design of the high-speed propelled experimental flight test vehicle HEXAFLY. In: *20th AIAA International Space Planes and Hypersonic Systems and Technologies Conference,* Glasgow, Scotland, 6-9 July: AIAA-2015-3539.

[5] Voevodenko, N.V., A.A. Gubanov, D.S. Ivaniushkin, V.Yu. Lunin, D.Yu. Gusev, M.A. Ivankin, V.A. Talyzin, and V.A. Yakovleva. 2015. Numerical and experimental studies of the flow on HEXAFLY-INT experimental flight test vehicle air intake. In: *20th AIAA International Space Planes and Hypersonic Systems and Technologies Conference,* Glasgow, Scotland, July 6 – 9: AIAA 2015-3584.

[6] Steelant, J., V. Villace, M. Marini, G. Pezzella, B. Reimann, S.L. Chernyshev, A.A. Gubanov, V.A. Talyzin, N.V. Voevodenko, N.V. Kukshinov, A.N. Prokhorov, A.J. Neely, C. Kennell, D. Verstraete, and D. Buttsworth. 2016. Numerical and experimental research on aerodynamics of high-speed passenger vehicle within the HEXAFLY-INT Project. *30th Congress of the International Council of the Aeronautical Sciences (ICAS),* Daegeon, Korea, September 26 – 30.

[7] Voevodenko, N.V., A.A. Gubanov, D.Yu. Gusev, M.A. Ivankin, D.S. Ivanyushkin, V.Yu. Lunin, P.A. Meshennikov, V.A. Talyzin, Yu.G. Shvalev, and V.A. Yakovleva. 2016. Boundary layer state influence on start of the inward-turning intake. In: *30th Congress of the International Council of the Aeronautical Sciences (ICAS),* Daegeon, Korea, September 26 – 30.